PERGAMON

Journal of Structural Geology 23 (2001) 1187–1202

JOURNAL OF STRUCTURAL GEOLOGY

www.elsevier.nl/locate/jstrugeo

Experimental investigation into the microstructural and mechanical evolution of phyllosilicate-bearing fault rock under conditions favouring pressure solution

B. Bos*, C.J. Spiers

HPT Laboratory, Institute of Earth Sciences, Utrecht University, PO Box 80021, 3508 TA Utrecht, the Netherlands

Received 1 June 2000; accepted 21 November 2000

Abstract

Mature crustal fault zones are known to be zones of persistent weakness. This weakness is believed to result from microstructural modifications during deformation, such as grain-size reduction and foliation development. Around the brittle–ductile transition, phyllosilicates are expected to have a significant effect on fault strength, in particular under conditions favouring pressure solution. To study such effects, we performed rotary shear experiments on brine-saturated halite/kaolinite mixtures, aimed at investigating the relation between microstructural and mechanical evolution in a system where pressure solution and cataclasis dominate. The results show significant strain weakening, and a transition with progressive strain towards more rate-sensitive and less normal stress-sensitive behaviour. This was accompanied by a microstructural evolution from a purely cataclastic microstructure to a mylonitic microstructure consisting of elongate, asymmetric clasts in a fine-grained, foliated matrix. The results demonstrate that strain weakening and the development of a typical 'mylonitic' microstructure can occur as a consequence of grain-size reduction by cataclasis, and a transition to pressure solution accommodated deformation, even in the absence of dislocation creep. The data raise questions regarding the reliability of microstructures as rheology indicators, as well as on the use of low strain, monomineralic flow laws for modelling crustal dynamics.

Keywords: Microstructure; Pressure solution; Mylonites; Halite; Phyllosilicates

1. Introduction

It has long been recognized that mature crustal fault zones are persistent zones of weakness, exerting a strong influence on crustal dynamics. One of the causes of the persistent weakness of such fault zones relative to the surrounding rock is believed to lie in microstructural changes during shear leading to strain weakening (Etheridge and Wilkie, 1979; White et al., 1980). These changes include grain-size reduction by processes such as cataclasis, dynamic recrystallization and mineral reactions, as well as the development of a foliation.

At depths below the brittle–ductile transition, grain-size reduction by dynamic recrystallization is widely thought to lead to weakening and localization as a result of a switch in deformation mechanism from dislocation creep to diffusion creep (Rutter and Brodie, 1988). However, the feasibility of major weakening by this has recently been questioned, at least for monomineralic materials (De Bresser et al., 1998). Moreover, recent numerical modelling studies show that permanent localization of deformation by this mechanism is possible only for very specific conditions, i.e. specific values of strain rate and cooling rate (Braun et al., 1999). In the case of brittle/frictional faulting and cataclasis, grain-size reduction, microcrack damage, cohesive strength loss and localization are inherent in the faulting process. In addition, grain-size reduction by cataclasis can lead to enhanced production of weak phyllosilicate minerals, in particular under the hydrothermal conditions of the brittle–ductile transitional region (e.g. Janeke and Evans, 1988; Wintsch et al., 1995).

Especially in phyllosilicate-bearing rocks the formation of a foliation may strongly influence the evolution of fault strength with strain. In crustal fault zones, phyllosilicates are ubiquitous (White et al., 1980; Passchier and Trouw, 1996; Snoke et al., 1999), either inherited from the host rock or formed as a retrograde alteration product (Wintsch et al., 1995). Under the conditions pertaining around the brittle–ductile transition, phyllosilicates are expected to be the weakest phase present (Logan and Rauenzahn, 1987; Shea and Kronenberg, 1993), and hence the presence and

* Corresponding author. Tel.: +31-302534976; fax: +31-302537725.
E-mail address: bbos@geo.uu.nl (B. Bos).

0191-8141/01/$ - see front matter
PII: S0191-8141(00)00184-X

alignment of phyllosilicates may have a significant influence on fault strength. Related to this, phyllosilicates are believed to increase grain boundary diffusion rates (Rutter, 1983; Hickman and Evans, 1995; Renard et al., 1997; Farver and Yund, 1999), enhancing diffusional mass transfer processes and further foliation development (Means and Williams, 1972). In addition, the presence of phyllosilicates at grain boundaries inhibits grain growth, thus stabilizing fine grain sizes (Etheridge and Wilkie, 1979; Olgaard and Evans, 1988), and retards grain contact healing processes (Hickman and Evans, 1995; Bos and Spiers, 2001). This may enhance deformation of fine-grained fault rocks by pressure solution-accommodated grain boundary sliding (Rutter and Mainprice, 1979; Lehner and Bataille, 1984/85; Paterson, 1995), allowing ductile deformation under conditions where dislocation creep is not yet possible. Despite this perceived importance of phyllosilicates in determining fault rheology in the brittle–ductile transitional region, there have been few experimental studies on their influence on fault constitutive behaviour under hydrothermal conditions.

In a previous study (Bos et al., 2001) we reported rotary shear experiments performed on simulated, gouge-bearing faults under conditions favouring pressure solution. These experiments were carried out using brine-saturated mixtures of halite (NaCl) and kaolinite as a rock analogue. At high slip velocities the experiments showed frictional, nearly rate-independent behaviour. For clarity, we emphasize that we understand the term 'frictional' to mean simply that shear stress is linearly related to normal stress, and not to imply any mechanistic interpretation. At low velocities frictional-viscous behaviour was observed, i.e. behaviour in which the shear stress is both normal stress and strongly shear strain rate dependent. Apparent friction coefficients down to 0.18 were recorded at the lowest sliding velocities. The microstructures observed after deformation showed asymmetric, sigmoidal halite clasts embedded in a strongly foliated, very fine-grained halite/kaolinite matrix. However, since all experiments involved slip rate and/or normal stress stepping sequences, it was not possible to directly relate microstructural development to mechanical behaviour. The microscale mechanisms leading to the observed behaviour therefore remained unclear to some extent, as did the applicability to natural fault zones.

The aim of the present work is to examine the relation between microstructural evolution and mechanical behaviour of simulated fault rock under conditions where pressure solution and cataclasis dominate over dislocation creep, thus simulating the brittle–ductile transition. We present mechanical data and microstructures obtained in a series of rotary shear experiments on simulated halite/kaolinite gouge. Samples were sheared to different strains, at velocities corresponding to both the frictional, rate-insensitive and the frictional-viscous regime as observed by us. The results show significant strain weakening, in particular at low sliding velocities. With increasing strain, a gradual transition from nearly rate-independent behaviour to frictional-viscous behaviour was observed. This was accompanied by microstructural evolution from a typical cataclasite at low strain to a strongly foliated, mylonitic fault rock at high strain. These results show that mylonitization and fault weakening may occur due to cataclasis and pressure solution, even in the absence of dislocation creep processes.

2. Experimental method

Synthetic gouges were prepared by mixing analytical grade, granular halite with very fine-grained kaolinite, in proportions of 3:1 by weight. This composition was chosen because the effect of sliding rate on strength observed in previous experiments (Bos et al., 2001) was strongest at this composition. The grain-size distribution of the halite was determined using a Malvern particle sizer. This showed the median grain size to be 104 μm, with 90% of the grains in the range 57–110 μm. The kaolinite was mostly submicron, with occasional grains of ~10 μm. Brine saturated with respect to the gouge material was used as a pore fluid, maintained at atmospheric pressure during the experiments.

The experiments were performed at room temperature, using the rotary shear apparatus shown schematically in Fig. 1. In this apparatus, the annular sample is sheared between two stainless steel 'wall rock' rings at controlled normal stress and sliding velocity (i.e. shear strain rate). Fig. 1 illustrates the experimental set-up. The toothed stainless steel 'wall rock' rings of 10 cm outer diameter and 1 cm width sandwich a layer of granular gouge (starting thickness after dry compaction ~750 μm). The sample is sealed with inner and outer stainless steel sealing rings, fitted with O-rings. Two diametrically mounted tubes in the outer sealing ring allow evacuation of the sample and addition of pore fluid. The stainless steel rings are gripped between two cylindrical forcing blocks. While the upper block is held fixed, the lower forcing block is rotated at controlled angular velocity by a motor plus gearbox, thus leading to shear on the synthetic fault. An Instron 1362 loading frame is used to apply and control normal stress to within 0.01 MPa. Shear stress on the fault is measured (resolution 0.005 MPa) using two strain gauge force gauges mounted in a torque couple which provides the reaction needed to hold the upper forcing block stationary. A Linear Variable Differential Transformer (LVDT, 1 mm full scale, 0.01% resolution) located inside the upper forcing block perpendicular to the sliding direction allows measurement of gouge compaction/dilatation normal to the shear plane. Rotary displacement is measured using a potentiometer geared to the rotation of the lower forcing block. O-ring friction was measured in a calibration experiment performed with water trapped between the wall rock rings (so the fluid pressure equalled the normal stress), and was found to contribute less than 0.01 MPa to the shear stress at fluid pressures below 3 MPa.

The experiments performed are listed in Table 1. In

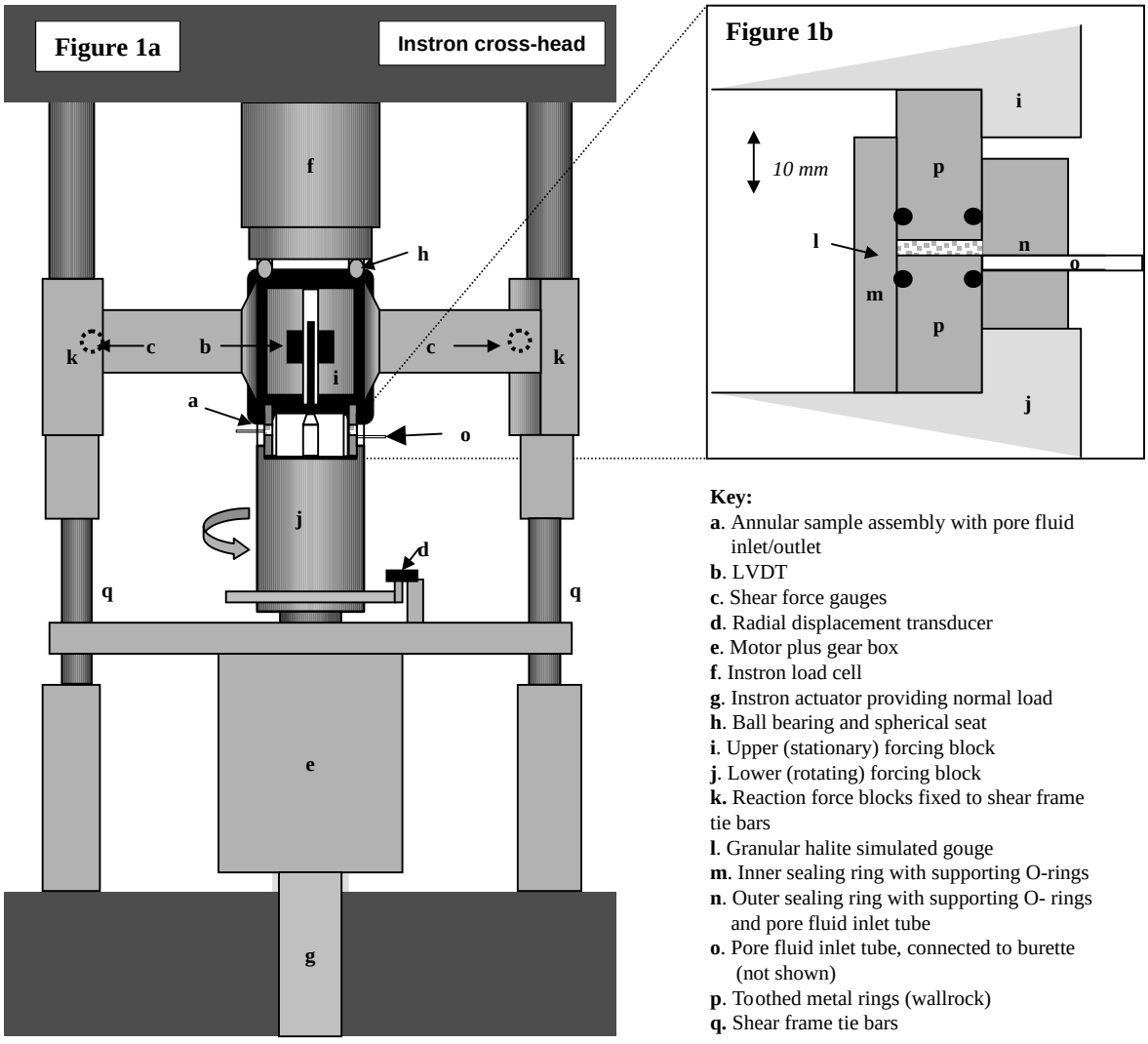

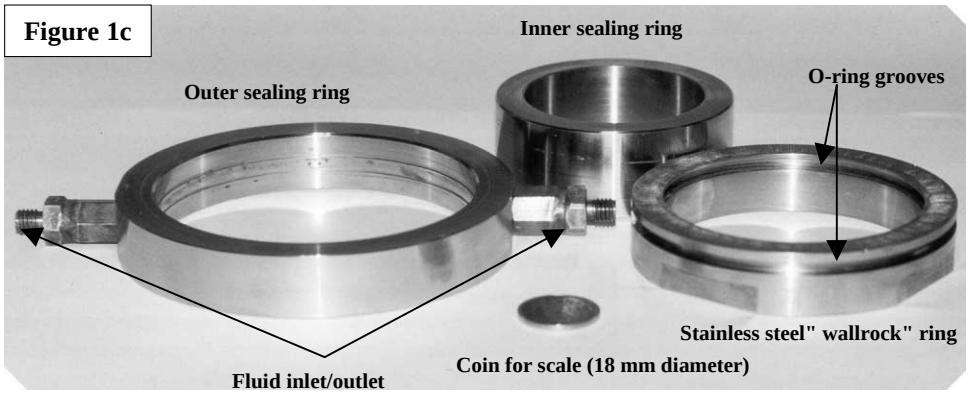

Fig. 1. Schematic diagram of (a) the deformation apparatus (not to scale) and (b) the sample assembly. (c) Photograph of one of the stainless steel toothed rings and inner and outer sealing rings. The diameter of the coin (for scale) is 18 mm.

setting up individual tests, the granular halite and kaolinite were mixed manually, and a pre-weighed quantity of gouge was evenly applied to the lower wall rock ring. The upper wall rock rings and the sealing rings were then assembled, thus completing the sample assembly which was next located between the forcing blocks. All samples were then compacted dry at 1 MPa for 10 min, to produce a gouge with a reproducible starting microstructure. Subsequently, the samples were unloaded and evacuated, and the saturated brine pore fluid was added. The required normal stress and

Table 1
List of experiments

Experiment	Gouge composition (halite/kaolinite ratio)	Normal stress (MPa)	Sliding velocity ($\mu m\ s^{-1}$)	Total displacement (mm)
str1	3:1	5	5	5.67
str2	3:1	5	5	12.34
str3	3:1	5	5	51.48
str4	3:1	5	0.2	0.87
str5	3:1	5	0.2	3.87
str6	3:1	5	0.2	17.41
str7	3:1	5	0.2	52.26
str8	3:1	5	0.2	536.38
str9	3:1	5	0.05	15.36
str10	3:1	2.5	0.2	14.69
str11	3:1	7.5	0.2	14.84

sliding velocity were then imposed. Eight experiments (str1–str8, see Table 1) were performed with the primary purpose of investigating the evolution of microstructure with strain. Three of these were performed at 5 $\mu m\ s^{-1}$ sliding velocity ('fast' experiments), which is well inside the rate-insensitive regime as reported by Bos et al. (2000a). The remaining five were performed at 0.2 $\mu m\ s^{-1}$ ('slow' experiments), which is well inside the strain-rate-sensitive regime. All of these experiments were performed at 5 MPa normal stress, reaching displacements given in Table 1. In addition, three experiments were performed in order to provide additional data on the evolution of mechanical behaviour (i.e. the strain rate and normal stress dependence of shear strength) with progressive strain. Two of these (experiments str10 and str11) were performed at a sliding velocity of 0.2 $\mu m\ s^{-1}$ and a normal stress of 2.5 and 7.5 MPa, respectively. Finally, experiment str9 was performed at 5 MPa normal stress and at 0.05 $\mu m\ s^{-1}$ sliding velocity.

The experiments were terminated by halting sliding and removing the normal load. The sample assembly was then removed from the forcing rings, and the samples were carefully extracted from the stainless steel wall rock rings. Subsequently, the samples were dried and impregnated with a transparent epoxy resin. Standard thin sections were cut normal to the sliding plane and parallel to the sliding direction, and inspected in plane polarized light using an optical microscope. In one sample (str7), the orientation distribution of crystallographic axes was measured by means of electron backscatter diffraction (EBSD). EBSD patterns of halite grains were determined on a Philips XL30FEG scanning electron microscope (SEM).

3. Results

3.1. Mechanical data

Fig. 2(a) shows the shear stress versus displacement data obtained from the microstructural evolution experiments (experiments str1–str8, see Table 1). The termination point of each experiment is marked with an arrow plus the number of the micrograph illustrating the corresponding microstructure. The experiments performed at 5 $\mu m\ s^{-1}$ ('fast' experiments, rate-insensitive regime) showed an initial shear stress peak, followed by minor weakening towards a steady state value of ~3.25 MPa (apparent friction coefficient μ of 0.65). The experiments run at 0.2 $\mu m\ s^{-1}$ ('slow' experiments, rate-sensitive regime) show a shear stress peak at ~3 mm displacement, after which significant strain weakening was observed. The weakening rate decreased with increasing displacement, the shear stress reaching a value of ~2.4 MPa at 10–20 mm displacement. The approach to this steady state was accompanied by an evolution from stable sliding to behaviour showing regular strength oscillations. These oscillations were characterized by a time period of ~15 min and an amplitude of up to 0.1 MPa. Although a quasi-steady state was reached after ~10–20 mm displacement, minor weakening continued throughout the experiment. The mechanical data obtained in the experiment to 538 mm displacement (str8) were affected beyond 70 mm displacement by misalignment of the forcing rings, leading to increased O-ring friction and unreliable shear stress measurements. For this reason the data from this experiment are not shown beyond 60 mm displacement.

Fig. 2(b) shows representative curves of compaction versus displacement for the fast and slow microstructural evolution experiments run to 50 mm displacement. All curves showed an initial rapid compaction stage, followed by a period of minor dilatation, corresponding to the peak stress in Fig. 2(a). After this, compaction resumed. The total amount of compaction for a given displacement was always larger in the 'slow' experiments.

Fig. 3 shows the mechanical data obtained from experiments str10 and str11 performed at a normal stress of 2.5 and 7.5 MPa at 0.2 $\mu m\ s^{-1}$ sliding velocity, as well as from experiment str9, performed at 5 MPa normal stress and at 0.05 $\mu m\ s^{-1}$ sliding velocity. All of these conditions fall in the rate-sensitive regime (Bos et al., 2001). Data from

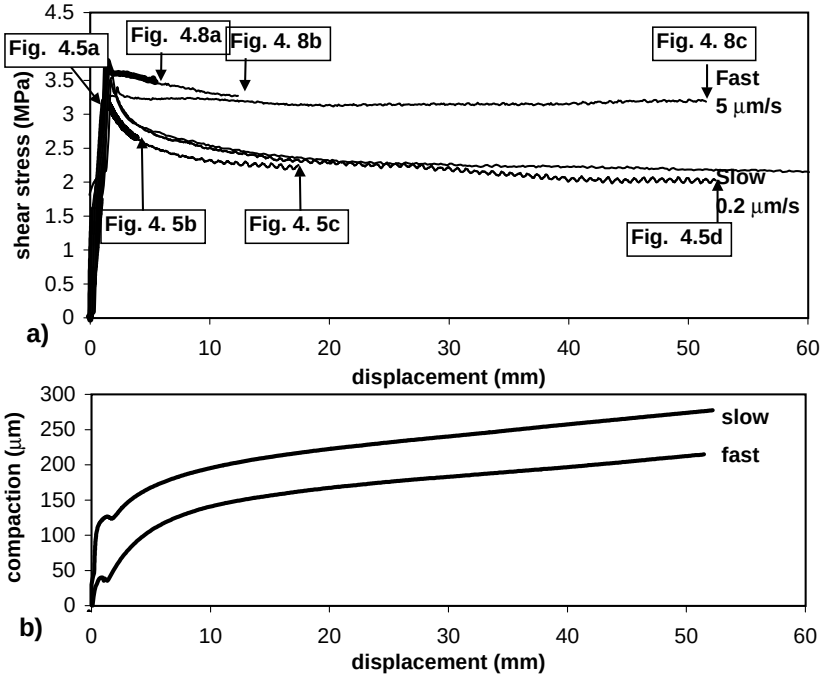

Fig. 2. (a) Shear stress versus displacement for experiments str1–str8, conducted to investigate the microstructural evolution. The points at which the respective experiments were halted are denoted with arrows, and the figure showing the corresponding microstructure is indicated. Note the significant strain weakening in the slow experiments, and relatively minor strain weakening in fast experiments. (b) Representative compaction versus displacement data (curves shown for experiments str3 and str7).

experiment str6 (2 μm s^{-1} sliding velocity, 5 MPa normal stress), which was also shown in Fig. 2(a), are shown for comparison. These experiments all show an initial stress peak, followed by on-going strain weakening, although quasi-steady state was reached after ~10 mm displacement. The data indicate that fault strength increased with increasing normal stress and sliding velocity at all strains.

In Fig. 4, the data presented in Fig. 3 have been used to illustrate the evolution of rheological behaviour with strain. Fig. 4(a) shows shear stress versus normal stress at a given shear displacement. The data show a significant normal stress dependence of shear stress at all shear displacements. From Fig. 4(a), the apparent friction coefficient, defined as the slope of a best-fit line through the data at a given shear displacement, was calculated. The term 'apparent' is used because the mechanical behaviour is not only normal stress dependent, but also strongly sliding rate dependent. Fig. 4(b) shows the calculated apparent friction coefficient as a function of displacement. The data clearly show that the normal stress sensitivity was highest immediately after the peak stress was reached, and gradually dropped off with increasing displacement. The largest change in apparent friction coefficient occurred in the first 10 mm of the experiment, i.e. during the strong strain weakening phase. In addition, Fig. 4(c) shows shear stress versus sliding velocity. These data show that shear stress increases with sliding rate at all displacements, with the dependence being strongest at higher displacements. The sliding rate sensitivity exponent *m*, defined as the slope of a linear best-fit line through the data shown in Fig. 4(c) for a

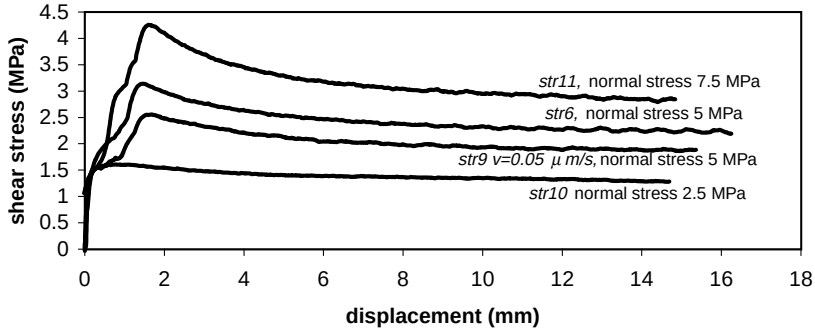

Fig. 3. Shear stress versus displacement for the experiments str9–str11 conducted to investigate mechanical behaviour evolution. Note evidence for clear dependence of shear stress on both normal stress and sliding velocity.

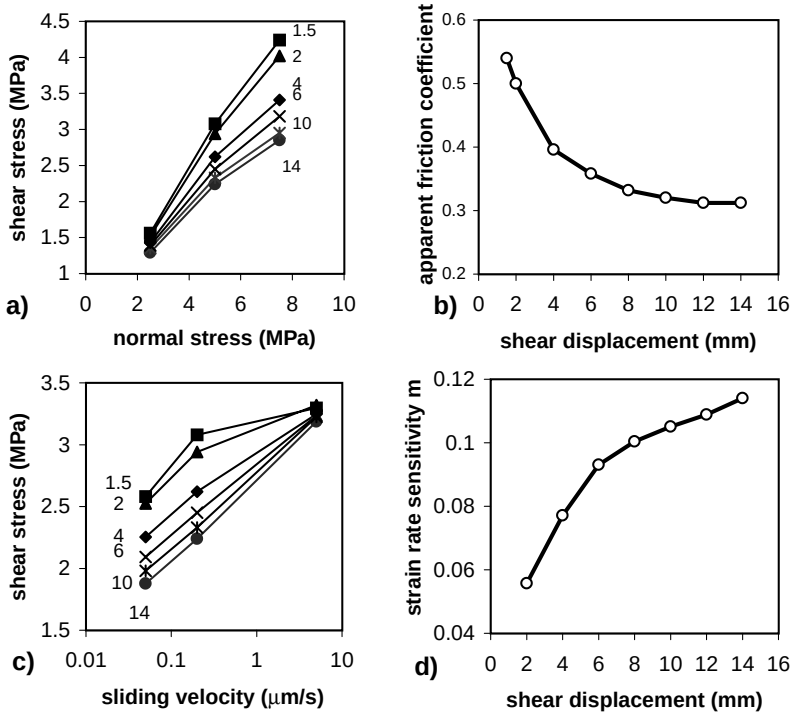

Fig. 4. Data showing mechanical evolution. (a) Shear stress versus normal stress, shear displacement as indicated. (b) Apparent friction coefficient μ (i.e. the slope of a linear fit through data of (a) at a given displacement) as a function of shear displacement. (c) Shear stress versus shear strain rate, shear displacement as indicated. (d) Strain rate sensitivity m (i.e. the slope of a linear fit through data of (c) at a given displacement) as a function of shear displacement.

given displacement, is shown in Fig. 4(d). It is evident from this that, for the first 2 mm displacement, the fit of a linear relation through the shear stress versus log sliding rate data is poor. Nevertheless, the sliding rate sensitivity gradually increases with increasing shear displacement. Overall, the data of Fig. 4 show an evolution from frictional, nearly rate-independent behaviour just after the peak stress to frictional-viscous (i.e. both normal stress and strain rate dependent) behaviour with increasing strain. This change is most rapid in the initial 10 mm of the experiments.

3.2. Microstructural evolution

3.2.1. Slow experiments

The microstructural evolution with progressive strain in the 'slow' experiments (i.e. at 0.2 μm s^{-1}) is shown in Fig. 5(a)–(e). Also indicated in each figure is the total shear strain, defined as the ratio of final displacement and final sample thickness. Additional details are shown in Fig. 6. Fig. 5(a) shows the microstructure of a sample from an experiment that was halted at the stress peak (experiment str4). The sample shows numerous intragranular fractures in the halite grains. No preferred alignment of clay particles was observed, but the halite particles seem to define a weak subhorizontal grain shape fabric. Also, most of the intragranular fractures are subvertical.

The microstructure observed midway through the rapid strain weakening stage following the peak stress is shown in Fig. 5(b) (experiment str5). A strong foliation has developed at ~35–40° to the imposed shear plane (rotations are measured counter-clockwise). The foliation is defined by elongated halite clasts, separated by anastomosing kaolinite bands. Several large halite clasts show intragranular fractures normal to the foliation. The foliation is transected by clay-rich synthetic shear bands (see white arrow in Fig. 5b), oriented at −35° to the imposed shear plane. These shear bands have an apparent right lateral shear sense, similar to the macroscopic fault.

Fig. 5(c) was taken after the rapid strain weakening stage (experiment str6), immediately after the onset of shear stress oscillations (refer to Fig. 2a). Strong grain-size reduction has occurred with respect to Fig. 5(b). The gouge material now consists of asymmetric remnant clasts in a fine-grained, foliated halite/kaolinite matrix. The sigmoidal clasts are generally oriented with their long axis at 25–35° to the shear zone boundary. In the clasts, intragranular fractures are again common. The foliated matrix, of which a detail is shown in Fig. 6(a), consists of elongate 'ribbon-like' halite grains separated by interconnected kaolinite bands. Measuring the area fraction occupied by clasts (i.e. halite grains with smallest axis larger than 10 μm) and matrix, by box-counting, showed that about 15% of the sample volume consists of clasts. Along the slip direction, regions rich in clasts were found to alternate with clast-poor regions. In the clast-rich regions the foliation is oriented at ~45° to the shear zone boundary, whereas in the clay-poor regions the foliation tends toward horizontal.

The microstructure obtained after ~52 mm (experiment str7) displacement is shown in Fig. 5(d). This microstructure

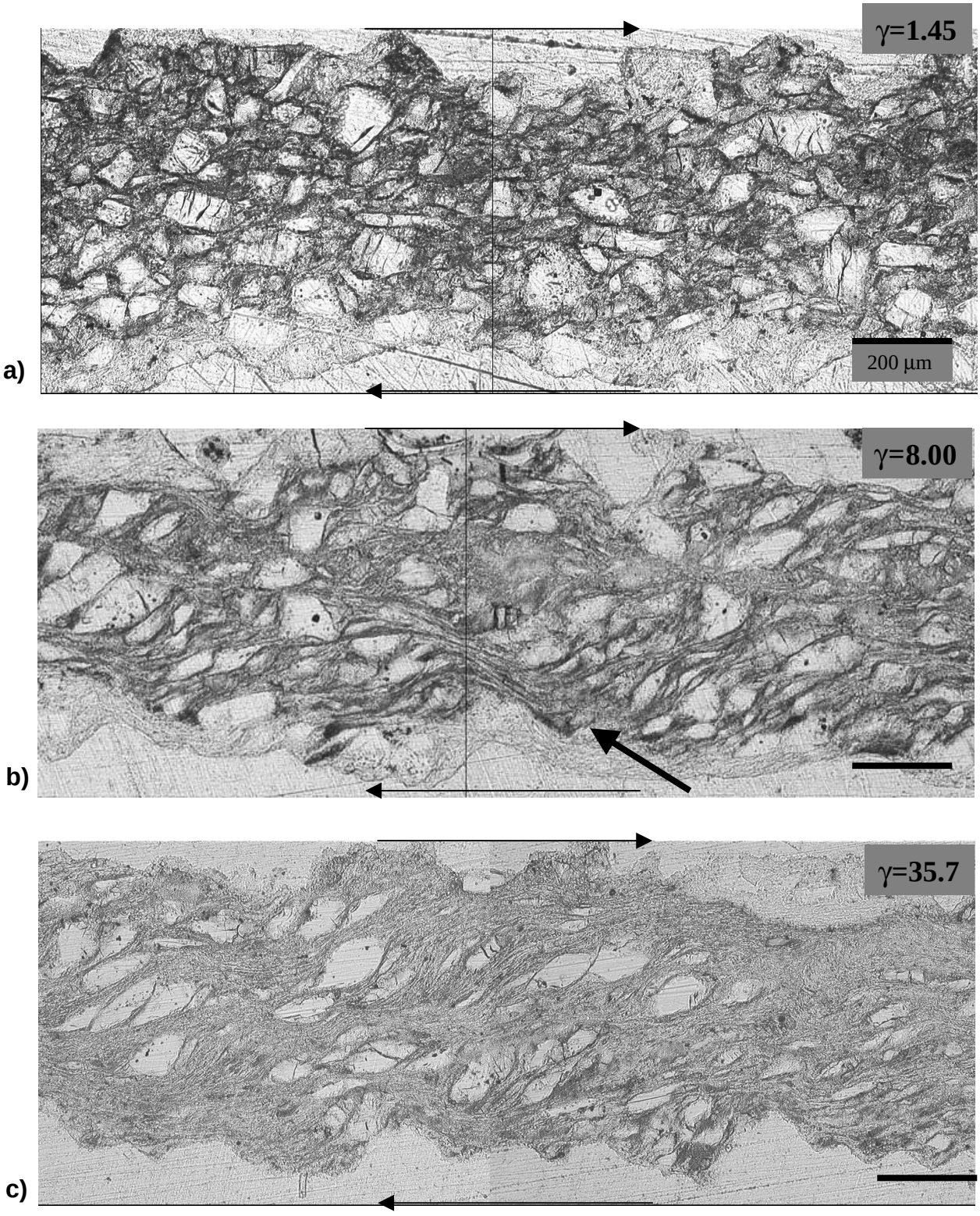

Fig. 5. Microstructures of samples deformed at 0.2 μm s^{-1} ('slow'). Shear sense is dextral, the scale bar is 200 μm in all figures. The accumulated shear strain is indicated at the top right. In all figures, the large light grains are halite, the darker material is kaolinite, of which the individual grains are too small to be seen. At the top and bottom of the samples, the teeth forming the surface roughness can be seen. (a) Microstructure at the shear stress peak. Note numerous intragranular fractures in halite and absence of foliation. (b) Microstructure during pronounced strain weakening. Note strong foliation, transected by clay-rich shear band (arrow), with dextral shear sense. (c) Microstructure after the strong weakening. Halite clasts are embedded in a fine-grained matrix (see detail in Fig. 6a). (d) Microstructure after 50 mm displacement. Note isolated asymmetric clasts with long tails, embedded in a fine-grained matrix. (e) Microstructure after 500 mm displacement. Note oblique foliation and absence of clasts.

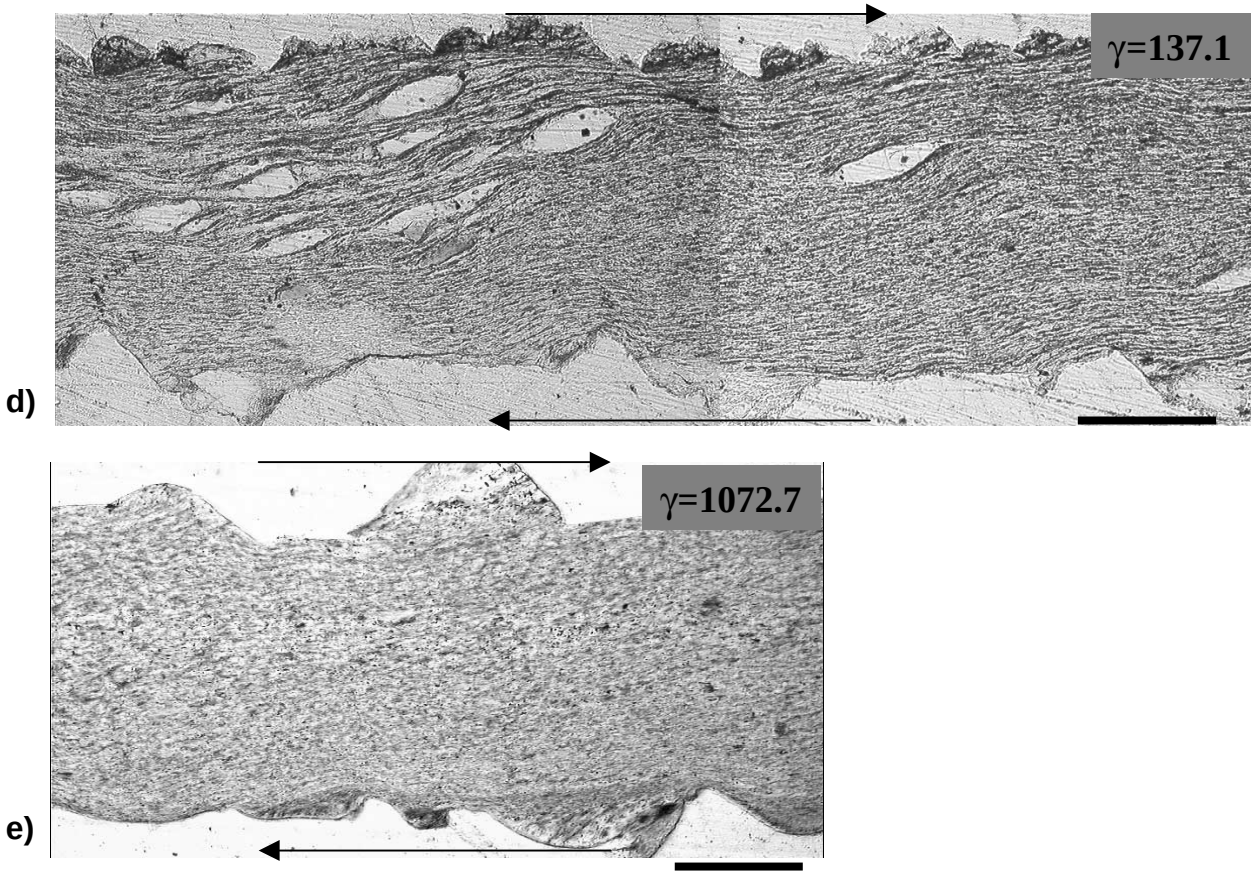

Fig. 5. (*continued*)

is similar to that shown in Fig. 5(c) in that the material consists of halite clasts in a fine-grained matrix. However, with accumulating strain the proportion of clasts has decreased to 4.4%. The clasts (see Fig. 6b for details) are now elongate, stair-stepping sigma objects (Passchier and Trouw, 1996), showing long tails. Most clasts appear free of intragranular cracks, but some are fractured, as shown in Fig. 6(c). In such cases, although the clast shape is still discernible, the fractures between the different fragments are already filled with kaolinite. The foliation, as defined by the matrix, shows a wavy trend, being more inclined to the shear plane in clast-rich regions than in clast-free regions.

Fig. 5(e) shows the microstructure obtained after ~500 mm displacement (experiment str8). The entire sample now consists of the fine-grained matrix described above, and no clasts are present. Note that the matrix grain size has not become significantly reduced compared to Fig. 5(c). The foliation is generally oriented at an angle of ~20° to the shear zone boundary, although locally the foliation is more nearly horizontal.

Electron backscatter diffraction was used to determine the crystallographic orientation of the halite ribbons in the matrix of sample str7 (cf. Fig. 5d). Fig. 7 shows equal area pole figures of ⟨100⟩, ⟨110⟩ and ⟨111⟩. The distribution of crystallographic axes is essentially random in this sample, i.e. no significant preferred orientation was observed.

3.2.2. 'Fast' experiments

The microstructural evolution in the 'fast' experiments (i.e. those performed at 2 μm s^{-1} and therefore in the rate-insensitive regime) is illustrated in Fig. 8(a)–(c). Fig. 8(a) shows a sample arrested just before the peak stress (experiment str1). Some intergranular cracks are visible in the blocky halite grains. No foliation or grain shape fabric was observed. Fig. 8(b) shows the sample after ~12 mm displacement (experiment str2), i.e. after minor strain weakening had occurred. The microstructure looks similar to Fig. 8(a) in that no foliation or grain shape fabric is present, but the average grain size is decreased significantly. Intragranular cracks are common in halite grains. Fig. 8(c) shows the sample after ~51 mm displacement (experiment str3). As in the 'slow' sample after 12 mm displacement (see Fig. 5c), large rounded halite clasts are now embedded in a fine-grained foliated matrix, but in general the grains are less elongate than in the slow experiment and lack the distinctive tails observed in the slow experiments. In all 'fast' samples, imprints of the teeth of the wall rock rings are still clearly visible at the top of the samples, but not at the lower side. The lower side shows a flat, subhorizontal surface where the sample came apart during sample retrieval from the apparatus. Fig. 9 shows details of the fine-grained matrix from sample str3. The microstructure is very similar to that observed in the 'slow' experiments

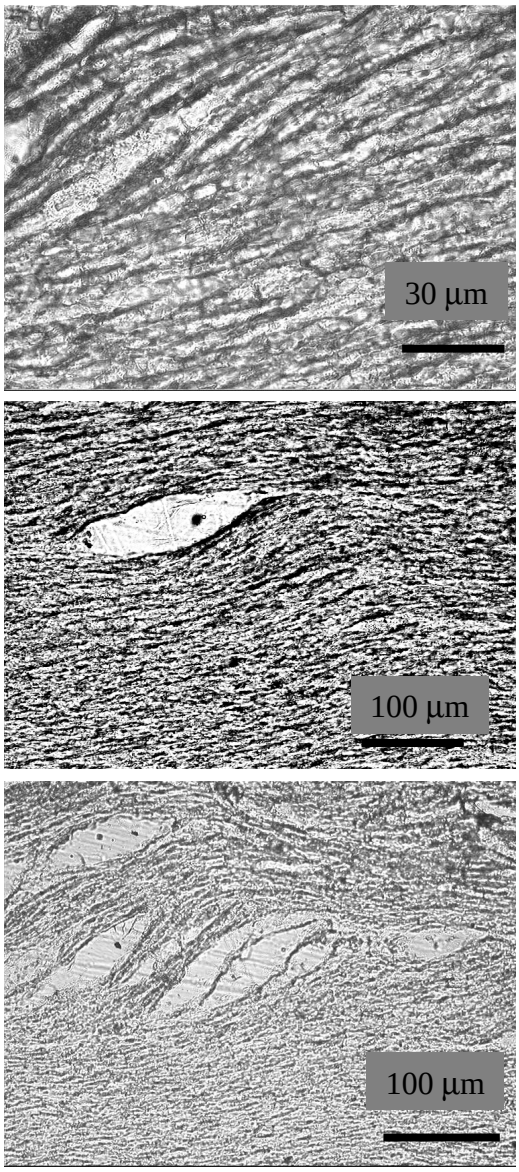

Fig. 6. Details of microstructures from the 'slow' experiments. Shear sense is dextral. (a) Detail of matrix, showing fine-grained intercalation of halite grains (light) and kaolinite layers (dark). (b) Example of asymmetric clast with elongate tail. (c) Detail of clasts showing evidence of fracture. The dark material separating the various clast fragments is kaolinite. Note the foliation wrapping around the clast.

(see Fig. 6a), in showing elongate, ribbon-like halite clasts surrounded by kaolinite. However, the foliation defined by the matrix is much more wavy in character than in the slow experiments, with orientations varying from subhorizontal to ~50° to the shear plane.

4. Discussion

4.1. Deformation mechanisms in our experiments

In this section, we will first discuss the mechanisms controlling fault strength at mechanical quasi-steady state in our experiments. Subsequently, we will address the mechanisms leading to the development of steady state and causing the observed transition in mechanical behaviour from predominantly rate-independent to frictional-viscous behaviour.

4.1.1. Deformation mechanisms versus microstructures at quasi-steady state

4.1.1.1. Slow experiments We have shown above that in the slow experiments (i.e. the experiments performed in the strongly rate-sensitive regime), the attainment of a quasi-steady state strength coincides with the development of a microstructure consisting of isolated sigma clasts embedded in a fine-grained, foliated matrix (see Fig. 5c and d). This microstructure is similar to that of natural *S–C* mylonites developed in natural rocks (White et al., 1980; Lister and Snoke, 1984) in that the orientation of the elongated matrix grains defines a mylonitic *S*-foliation, and the elongate tails of the clasts define a horizontal *C*-foliation (see Fig. 5d). The shape fabric of the clasts clearly does not track the finite strain ellipse (since this would be oriented at 1.7° and 0.4° to the shear plane in Fig. 5c and d, respectively). This implies that shear deformation was not homogeneously distributed over the clasts and the matrix. The fact that only minor weakening occurred in the slow experiments from 18 to 50 mm displacement, while the volume of remnant clasts was reduced by more than a factor 2 (cf. Fig. 5c and d) suggests that the matrix, and not the clasts, controlled fault strength. Indeed, in this displacement interval, the relative proportion of matrix increased from 80 to 95%, leading to a factor of 1.2 decrease in average matrix strain rate. Since gouge strength at this velocity is known to be roughly proportional to strain rate to the power 0.2 (Bos et al., 2001), this should have resulted in weakening by a factor of 1.04. This is in good agreement with our present data, which show weakening by a factor of 1.10 in the same displacement interval.

Focusing now on the matrix, it was observed that the foliation defined by the matrix also does not track the finite strain ellipse: the foliation was still at ~20° to the shear zone boundary at a shear strain of 1072 (see Fig. 5e), rather than the 0.05° of the finite strain ellipse. This shows that within the matrix, strain was not accommodated homogeneously, i.e. deformation did not simply involve grain flattening and rotation. In view of the expected low friction coefficient of kaolinite layers, especially in the presence of fluids, deformation might be envisaged to involve sliding along through-going foliation planes. For this to produce a foliation that is steeper than the orientation of the finite strain ellipse requires overall dilatation of the material (just as compaction would cause further flattening), whereas our data show compaction (cf. Fig. 2b) during the experiment. It should be noted, however, that the foliation in our materials is not defined by through-going kaolinite planes, but rather by

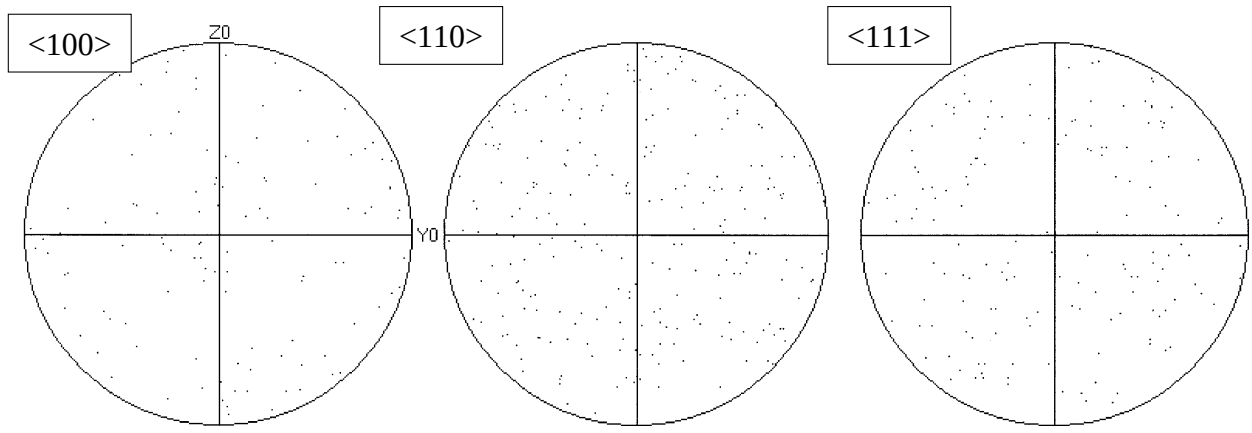

Fig. 7. Crystallographic preferred orientation plots, obtained using EBSD. A total of 40 matrix halite grains were measured. Pole figures are shown for the ⟨100⟩, ⟨110⟩ and ⟨111⟩ poles. The *z*-axis (vertical) and *y*-axis (horizontal) are perpendicular to the shear direction, the *x*-axis and *y*-axis define the shear plane. No significant lattice preferred orientation is present.

the long axes of elongate halite grains which are surrounded by an anastomosing network of kaolinite, as depicted schematically in Fig. 10. In this situation, no flat, through-going kaolinite planes are present. Rather, the kaolinite planes form interconnecting sinuous layers, and sliding along kaolinite layers must be accommodated on the grain scale to overcome local irregularities (i.e. the sinuosity of the kaolinite layers). We propose that deformation of the matrix material involved sliding along kaolinite foliae, accommodated by deformation of the halite grains.

The observation that the shear stress is strongly strain rate dependent in the 'slow' experiments implies the action of time-dependent deformation mechanisms in determining either the sliding strength of the kaolinite foliae or the creep strength of the deforming halite grains. Previous experiments have shown that kaolinite shows frictional, rate-independent behaviour under the conditions of our experiments (Bos et al., 2001), so the rate-dependent behaviour must be due to the mechanism of grain deformation. Possible rate-dependent deformation mechanisms are crystal plasticity, stress corrosion cracking and pressure solution creep. Previous work has shown that pure halite deforms by brittle mechanisms under the conditions of our experiments (Bos et al., 2000), and much higher normal stresses than those used in our experiments are needed to activate crystal plasticity (Shimamoto and Logan, 1986; Chester, 1988). In addition, the absence of any significant crystallographic preferred orientation in our samples (see Fig. 7) rules out a significant contribution of crystal plasticity to the observed behaviour. The absence of significant grain-size reduction in the matrix (cf. Fig. 5c–e) shows that cataclasis by stress corrosion cracking was of only minor importance (although it may well have contributed to converting large clasts into fine-grained matrix material in earlier stages of the experiment). By elimination, this leaves pressure solution as the dominant time-dependent grain deformation mechanism. This is supported by the microstructures, which show elongate tails on the larger grains, demonstrating that mass transfer occurs even on a scale larger than the matrix grain scale. In addition, it is known from compaction studies that pressure solution is rapid in halite aggregates under the conditions of our experiments (Spiers et al., 1990).

Deformation by grain boundary sliding along kaolinite foliae accommodated by pressure solution of halite grains would lead to steady state shearing behaviour by dissolution of material at the top right end of the grains (cf. Fig. 10) and redeposition at the lower left end. In this scenario, grain boundary sliding along kaolinite foliae and accommodation of sliding by grain deformation are serial processes, i.e. the slowest determines the overall rate of deformation. The observed mechanical behaviour, which showed that shear strength is both normal stress and sliding rate dependent, is consistent with this interpretation: in a situation where pressure solution and grain boundary sliding along kaolinite foliae operate at the same time, pressure solution will give rise to the sliding rate dependence, whereas the normal stress dependence is due to grain boundary sliding (which is a frictional process under the conditions investigated). A lower limit for fault strength is attained when accommodation by pressure solution is negligibly easy. In this case, the sliding friction of the kaolinite layers will determine fault strength.

4.1.1.2. Fast experiments At the high sliding velocity ($5\ \mu m\ s^{-1}$) only minor strain weakening occurred, with quasi-steady state established after ~10 mm displacement. The microstructures, which show evidence of significant grain-size reduction, suggest that at least up to shear strains of 19.2 the main deformation mechanism was cataclasis. The fact that the gouge showed overall compaction in this stage may indicate that the local dilatation accompanying cataclasis is counteracted by time-dependent compaction due to pressure solution. At higher strains (Fig. 7c), a foliation developed, in many respects similar to the low velocity experiments. The fact

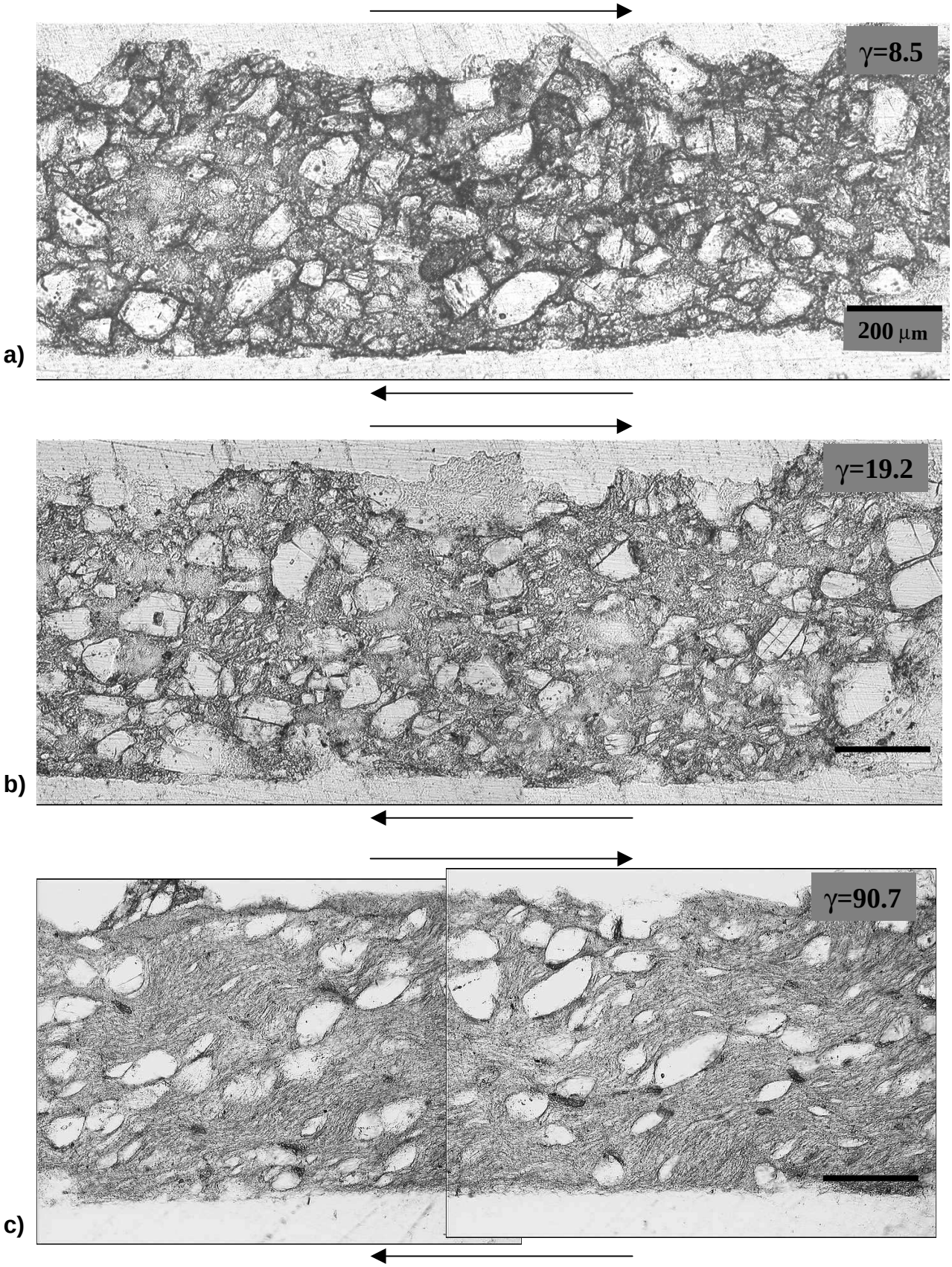

Fig. 8. Microstructures of samples deformed at 5 μm s^{-1} ('fast'). Note fractures in halite in (a) (str1) and (b) (str2), and foliation in (c) (str3).

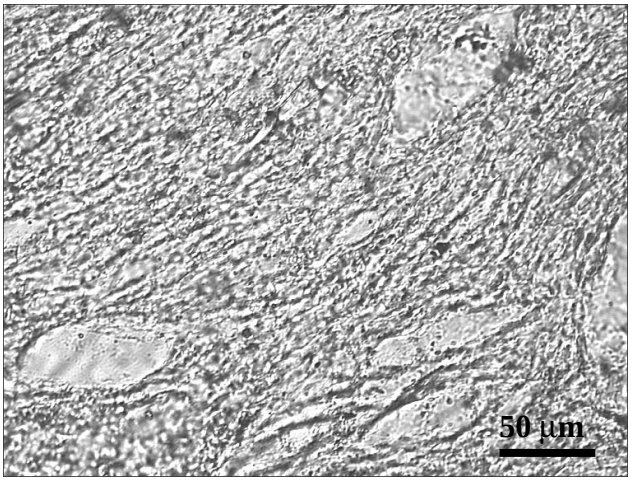

Fig. 9. Detail of matrix of Fig. 8(c) (sample str3). Note similarity to Fig. 6.

that the mechanical behaviour was nearly rate independent and linearly normal stress dependent suggests that shear deformation involved mainly time-independent processes. We propose that shear deformation at high strains occurred by sliding along or within kaolinite foliae, similar to the behaviour at low sliding velocity, but now accommodated by sliding of halite grains over each other, i.e. by sliding along the kaolinite-coated leading edges of the halite grains. This is consistent with the normal stress dependent, nearly rate-independent behaviour observed, since both sliding along kaolinite foliae and the dilatation accompanying sliding along the leading edges are normal stress dependent, time-independent processes. Finally, it should be mentioned that the subhorizontal lower surface of the sample suggests a contribution of localized sliding along this surface to total fault slip.

Although the microstructure changed significantly with strain in the 'fast' experiments, the strength and mechanical behaviour did not. This may be explained by the fact that both cataclasis (involving brittle fracture and dilatation) and sliding along kaolinite foliae accompanied by dilatation produce frictional, nearly rate-independent behaviour.

4.1.2. Evolution of mechanical behaviour with increasing strain

As discussed above, only minor strength evolution was observed in the fast experiments, in spite of the fact that there was significant microstructural evolution in these samples. Moreover, it is known from our previous experiments that the fast experiments are characterized by rate-insensitive sliding behaviour.

In contrast, the present slow experiments showed significant strain weakening after the initial stress peak, especially in the first 10 mm displacement. The data for these experiments show a transition with strain from frictional, nearly rate independent to strongly rate-dependent behaviour. The microstructures show that around the peak stress deformation must have occurred mainly by cataclasis, which explains the nearly rate-independent behaviour observed. After the peak stress, deformation becomes partitioned between clay-rich shear bands (Fig. 5b) and a developing oblique '*S*-foliation'. The shear bands are similar to the C'-type shear bands, also termed extensional crenulation cleavage often observed in natural mylonites (Platt and Vissers, 1980; White et al., 1980; Lister and Snoke, 1984; Platt, 1984; Passchier and Trouw, 1996). The sequence in which the *S*- and C'-foliation developed in our 'slow' experiments, and the partitioning of strain between them, remains unclear. We are now preparing see-through experiments on these materials to address this issue, the results of which will be reported in a separate paper. Our experiments seem to support the idea that these shear bands are associated with strain weakening (Platt and Vissers, 1980; Platt, 1984), but the actual weakening could also have been due to the development of the *S*-fabric.

Shimamoto and co-workers reported microstructures from deformation experiments on pure halite aggregates deformed in the semi-brittle field (Shimamoto, 1986, 1989; Shimamoto and Logan, 1986). These showed aligned trains of statically recrystallized grains forming an *S*-foliation, transected by discrete faults in the C' orientation. Shimamoto compared these to natural *S*–*C* mylonites (notably to the C' variety) and claimed that natural *S*–*C* mylonites may represent late stage localization and a transition from ductile to frictional behaviour, which he observed in his experiments. Our results are in direct contradiction with this interpretation. In our experiments, C'-type shear bands develop during strain weakening and a transition from nearly rate independent towards more ductile behaviour. Several explanations for this contradiction can be put

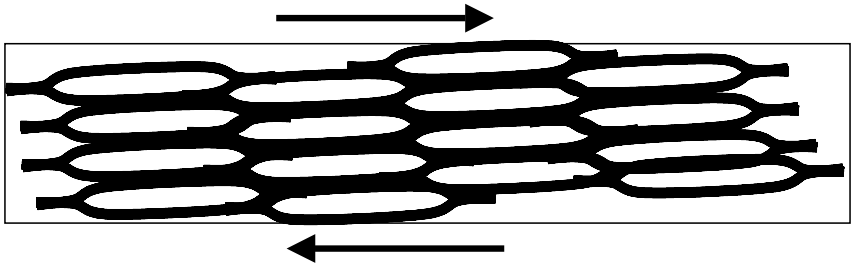

Fig. 10. Schematic depiction of microstructure of matrix, showing contiguous, anastomosing network of kaolinite layers (black) surrounding halite grains (white).

forward. The main differences between our experiments and those reported by Shimamoto are that: (1) Shimamoto's experiments are in a regime where (limited) dislocation creep is possible, and (2) Shimamoto's experiments were done on dry, clay-free samples. Given the fact that natural C'-type shear bands develop exclusively in phyllosilicate-bearing rocks, it seems that our samples would provide a better analogue for natural materials. However, this remains speculative.

On the basis of our own experiments, sliding along the *S*-foliation can be accommodated either on the grain scale, by dilatation or pressure solution, or on a larger scale, by the formation of sample-scale shear bands. The fact that shear bands were observed during the weakening phase indicates that at this stage accommodation of sliding by shear bands was easier than accommodation by grain scale mechanisms. With progressive displacement, cataclasis and intergranular sliding led to significant grain-size reduction and phase mixing, as illustrated in Fig. 6(c). Also, pressure solution led to strong elongation of halite grains, especially in the shear bands (note in this respect the strongly elongate halite grains in the shear band in Fig. 5b). This allowed formation with progressive strain of the fine-grained, foliated halite/kaolinite matrix. A fine grain size is expected to favour pressure solution creep processes, since these are strongly grain-size sensitive. Thus, as soon as an interconnected network of this matrix material had formed, it could start to accommodate a steadily increasing proportion of the sample-scale deformation by a mechanism such as described in the previous section. We propose that with increasing matrix proportion, accommodation of sliding on wavy planes forming the *S*-foliation by local pressure solution and dilatation became more favourable than the formation of sample-scale shear bands, so the basic requirement for the development of shear bands disappeared.

In summary, we conclude that in our 'slow' experiments the gradual transition in mechanical behaviour from frictional, nearly rate-independent behaviour to frictional-viscous behaviour with progressive strain was caused by a progressively decreasing role of cataclasis and an increasing role of pressure solution-accommodated intergranular sliding along/within kaolinite layers. In the fast experiments, a similar transition in mechanism took place, but the accommodation of sliding along kaolinite foliae occurred mainly by local dilatation, leading to rate-insensitive behaviour throughout the experiment.

4.2. Implications for natural fault rock

4.2.1. Fault weakening and localization by cataclasis plus solution transfer

Generally, microstructures like tailed porphyroclasts, ribbon grains, grain-shaped foliations and *S*–*C* fabrics are considered indications that crystal plastic deformation and dynamic recrystallization were dominant in the evolution of mylonites, and in bringing about shear localization. Our experiments show that *S*–*C* fabrics can be formed also under conditions where cataclasis and solution transfer are dominant over dislocation creep. The crystallographic preferred orientation patterns, which showed that the crystallographic axes were randomly oriented even in a sample that was deformed to a shear strain of 137, confirm that dislocation creep is unimportant in our experiments. Hence, crystal plastic deformation is not a necessary requirement for the formation of *S*–*C* fabrics, in spite of the fact that evidence for crystal plasticity is ubiquitous in natural *S*–*C* mylonites. The typical 'mylonitic' microstructures we observed did not develop in samples deformed under dry conditions (Bos et al., 2001), suggesting that solution transfer mechanisms play an important role in their formation (see also Means and Williams, 1972).

The present experiments provide an experimental account of a mechanism for the formation of weak fault rocks by a switch in deformation mechanism from nearly rate-independent behaviour to grain-size sensitive diffusional creep following grain-size reduction by cataclasis. This mechanism is distinct from the often-envisaged scenario of grain-size reduction by dynamic recrystallization, and is not subject to the criticisms regarding the possibility of a clear-cut mechanism switch from dislocation creep to diffusion creep and the limitations regarding the amount of weakening possible by such a switch (Etheridge and Wilkie, 1979; De Bresser et al., 1998; Ter Heege et al., 1999). The mechanism presented here is expected to be particularly important around the brittle–ductile transition, where both brittle processes and solution transfer processes are important. It can effectively lead to a shallowing of the brittle–ductile transition in zones of high strain, allowing deformation of the hydrated, fine-grained shear zone by a ductile mechanism whereas the country rock is still in the brittle field, as also proposed by Stewart et al. (2000) from field observations on the Great Glen Fault Zone. Since diffusional processes will rapidly obliterate microstructural evidence of cataclasis (such as angular grains and microcracks), the cataclastic nature of grain-size reduction may not always be apparent in natural rocks. Also, evidence for deformation by pressure solution may be easily overprinted by small amounts of dislocation creep. Hence, microstructures of fault rocks formed by a mechanism of cataclasis, followed by pressure solution creep accompanied by some dislocation creep may be very similar to those of mylonites formed purely by dynamic recrystallization.

4.2.2. Microstructure as a rheology indicator

An important use of microstructural observations in natural rocks is to constrain the operative deformation mechanisms, and thus the rheology of the deformed material. Our experiments suggest that this may be much more problematic than frequently thought.

As an example, compare our Figs. 5(c) and 8(c). In both figures, the material consists of rounded, elongate clasts in a fine-grained halite/kaolinite matrix. In general, the

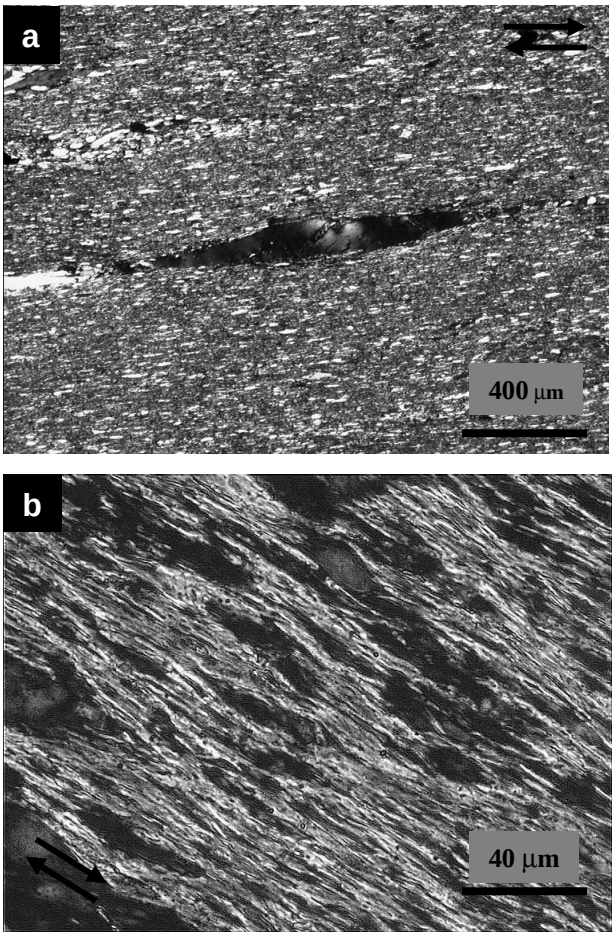

Fig. 11. Microstructures from mica-rich bands in a shear zone from the Barthelémy massif, French Pyrenees. Shear sense is dextral in both images, and images were taken with crossed polarizers. (a) Asymmetric clast in fine-grained, mica-rich matrix. (b) Fine-grained mixture of mica grains (light) and elongate quartz grains (dark). Note that in (b) the shear zone boundary is oblique to the horizontal of the image (see shear sense arrows at bottom left).

microstructures look very similar, although in Fig. 8(c) the clasts are more rounded than in Fig. 5(c). Also, the close-ups of the matrix (Figs. 6a and 9) show much similarity. However, the mechanical behaviour displayed by these samples is very different: Fig. 5(c) represents material deforming by a strongly strain rate sensitive mechanism, whereas the mechanical behaviour of the material depicted in Fig. 8(c) was nearly rate independent. Thus, very different rheologies are represented by very similar microstructures.

Furthermore, compare Fig. 8(b) and (c). Although the microstructures are very different, the mechanical behaviour was nearly rate independent in both cases, and no significant strength change occurred from Fig. 8(b) to (c). As argued above, the mechanism of deformation evolves from behaviour dominated by cataclasis in Fig. 8(a) to behaviour dominated probably by sliding along kaolinite foliae and accommodative dilatation in Fig. 8(c). Both these mechanisms produce nearly rate-independent, normal stress-dependent behaviour. Thus, very similar macroscopic fault rheologies may be associated with very different internal microstructures.

Lastly, Fig. 11(a) and (b) show microstructures from mica-rich strands in a natural shear zone from the Barthelémy massif, French Pyrenees. On thin-section scale, this shear zone shows an alternation of mica-rich and essentially mica-free bands. Fig. 11(a) shows an asymmetric clast in a fine-grained matrix mica-rich matrix. Fig. 11(b) shows details of a mica-rich band in the mylonite. Comparing these to our sample microstructures (in particular comparing Fig. 11a to Fig. 6b and Fig. 11b to Fig. 6a), the similarity in geometry is striking. In our samples, deformation occurred by a combination of intergranular sliding of halite grains along kaolinite foliae, local dilatation, and pressure solution. In the natural material, undulatory extinction evidences the operation of dislocation creep. Whether pressure solution and sliding also occurred in these samples is difficult to say. Evidence for the operation of pressure solution may have been obliterated by concurrent operation of other processes. In addition, it is impossible to deduce from the microstructure to what extent sliding along mica grains has occurred, since the local finite strain is not known. Our experimental data show that dislocation creep is not a requirement for producing this type of microstructure. Hence, in these natural samples the relative contributions of dislocation creep, intergranular sliding, and pressure solution creep to the total strain and to the rheology of the material are unclear.

We conclude that, especially in polyphase, phyllosilicate-bearing materials, where mixed deformation processes can occur, the microstructure may not be a very reliable tool for constraining rheology. Also, microstructure cannot be used for strain analysis in these materials, because of the large amount of intergranular sliding that may be involved.

4.2.3. Implications for crustal strength

A general feature observed in our experiments reported here and previously (Bos et al., 2001) is that the strength of the samples approaches the strength of the weakest phase present if strains significantly large for microstructural evolution to take place are accumulated. The evolution of the strength of a polymineralic aggregate towards the strength of the weaker phase has also been observed in experiments on aplite (Dell'Angelo and Tullis, 1996), orthopyroxene granulite (Ross and Wilks, 1996), calcite/halite mixtures (Price, 1982; Jordan, 1987; Kawamoto and Shimamoto, 1998), halite/anhydrite mixtures (Ross and Bauer, 1992), mica-bearing schists (Shea and Kronenberg, 1993) and many others. In modelling crustal tectonic processes, a strength profile is generally used with brittle behaviour represented by Byerlee's friction law and ductile/plastic behaviour represented by a flow law for pure quartz or feldspar (Goetze and Evans, 1979; Govers and Wortel, 1995; Ranalli, 1997), calibrated in low strain experiments.

However, crustal tectonic processes are for a large part controlled by the behaviour of high strain faults and shear

zones (either newly formed or inherited from earlier deformation), which often contain a significant proportion of phyllosilicates. These shear zones are likely to be significantly weaker than predicted using flow laws for monomineralic quartz or feldspar, and also significantly weaker than their undeformed counterparts (Janeke and Evans, 1988; Wintsch et al., 1995; Stewart et al., 2000). Also, by comparison with our experiments, it may very well be that the rheology of phyllosilicate-rich shear zones is both normal stress and strain rate sensitive. Additionally, fluid flow through fault zones may cause phyllosilicates to become concentrated in high-strain fault zones at the expense of more soluble minerals such as quartz and feldspar, in this way bringing fault strength closer to the intrinsic strength of phyllosilicates with increasing strain. From the above, we suggest that instead of using a classical brittle–plastic strength profile based on low strain, monomineralic materials, crustal rheology could be modelled by using the strength of the weakest major phase present. This idea has been put forward earlier by Shea and Kronenberg (1992), who also pointed out that around the brittle–ductile transition, the weakest phase will usually be mica.

With increasing depth (and hence temperature), quartz becomes weaker than mica because the activation energy for creep is higher for quartz than for mica (Mares and Kronenberg, 1993). One way of taking strain weakening into account would be to allow the rheology in a model to develop, in a realistically prescribed manner, from a quartz rheology to a mica rheology with increasing strain. Admittedly this is a very simplified approach, but it is surely more realistic than the strength envelopes now used, particularly for zones of high strain. While crustal deformation around the brittle–ductile transition surely exhibits additional complexities, we believe that incorporating mica strength into crustal rheology profiles will provide a significantly improved approximation to crustal strength in high strain zones.

5. Conclusions

Experiments were performed with the aim of investigating the relationship between microstructural evolution and mechanical behaviour. The following conclusions can be drawn:

1. We observed a transition in mechanical behaviour from nearly rate-independent behaviour at low strains to frictional-viscous behaviour at high strains. This transition was caused by the development with progressive strain of a fine-grained halite + kaolinite matrix, which accommodated deformation by a pressure solution-controlled mechanism.
2. Deformation of the halite + kaolinite matrix involved sliding of halite grains along kaolinite layers, accommodated by local pressure solution and/or dilatation. The combination of sliding along kaolinite layers and pressure solution probably gave rise to both normal stress and strain rate dependent strength.
3. The data suggest a mechanism of weakening and localization of deformation by grain-size reduction due to cataclasis, followed by a transition from brittle behaviour to pressure solution-accommodated creep of fault rock.
4. Our microstructures suggest that although microstructural evidence for crystal plasticity may be ubiquitous in natural mylonites, dislocation creep is not a necessary requirement for their development, and the relative contributions of dislocation creep and cataclasis + solution transfer to strain accumulation and fault strength are in general unclear.
5. Although microstructure may be useful as an indication for which deformation processes were active in a rock, using microstructure as a rheology gauge is problematic, especially in phyllosilicate-bearing rocks where combined deformation mechanisms occur.
6. Crustal strength in deforming regions may be modelled more realistically by using the strength of the weakest phase present, instead of applying the strength of quartz or feldspar throughout the strength envelope. At the brittle–ductile transition, the weakest phase will usually be mica.

Acknowledgements

Hans de Bresser and Jan ter Heege are thanked for discussions. Martyn Drury is thanked for assisting with the EBSD measurements. Colin Peach, Peter van Krieken, Gert Kastelein and Eimert de Graaff are thanked for technical assistance. Constructive comments by reviewers Andreas Kronenberg and Toshihiko Shimamoto and by the editor Jim Evans are greatly appreciated.

References

Bos, B., Peach, C.J., Spiers, C.J., 2000. Slip behavior of simulated gouge-bearing faults under conditions favoring pressure solution. Journal of Geophysical Research 105, 16699–16717.

Bos, B., Peach, C.J., Spiers, C.J., 2001. Frictional-viscous flow of simulated fault gouge caused by the combined effects of phyllosilicates and pressure solution. Tectonophysics 327, 173–193.

Bos, B., Spiers, C.J., 2001. Effect of phyllosilicates on fluid-assisted healing of gouge-bearing faults. Earth Planetary Science Letters 184, 199–210.

Braun, J., Chéry, J., Poliakov, A., Mainprice, D., Vauchez, A., Tomassi, A., Daignières, M., 1999. A simple parameterization of strain localization in the ductile regime due to grain size reduction: a case study for olivine. Journal of Geophysical Research 104, 25167–25181.

Chester, F.M., 1988. The brittle–ductile transition in a deformation-mechanism map for halite. Tectonophysics 154, 125–136.

De Bresser, J.H.P., Peach, C.J., Reijs, J.P.J., Spiers, C.J., 1998. On dynamic recrystallization during solid state flow: effects of stress and temperature. Geophysical Research Letters 25, 3457–3460.

Dell'Angelo, L.N., Tullis, J., 1996. Textural and mechanical evolution with progressive strain in experimentally deformed aplite. Tectonophysics 256, 57–82.

Etheridge, M.A., Wilkie, J.C., 1979. Grainsize reduction, grain boundary sliding and the flow strength of mylonites. Tectonophysics 58, 159–178.

Farver, J.R., Yund, R.A., 1999. Oxygen bulk diffusion measurements and TEM characterization of a natural ultramylonite: implications for fluid transport in mica-bearing rocks. Journal of Metamorphic Geology 17, 669–683.

Goetze, C., Evans, B., 1979. Stress and temperature in the bending lithosphere as constrained by experimental rock mechanics. Geophysical Journal of the Royal Astronomical Society 59, 463–478.

Govers, R., Wortel, M.J.R., 1995. Extension of stable continental lithosphere and the initiation of lithosphere scale faults. Tectonics 14, 1041–1055.

Hickman, S.H., Evans, B., 1995. Kinetics of pressure solution at halite–silica interfaces and intergranular clay films. Journal of Geophysical Research 100 (B7), 13113–13132.

Janeke, S.U., Evans, J.P., 1988. Feldspar-influenced rock rheologies. Geology 16, 1064–1067.

Jordan, P., 1987. The deformational behaviour of bimineralic limestone–halite aggregates. Tectonophysics 135, 185–197.

Kawamoto, E., Shimamoto, T., 1998. The strength profile for bimineralic shear zones: an insight from high-temperature shearing experiments on calcite–halite mixtures. Tectonophysics 295, 1–14.

Lehner, F.K., Bataille, J., 1984/85. Nonequilibrium thermodynamics of pressure solution. Pure and Applied Geophysics 122, 53–85.

Lister, G.S., Snoke, A.W., 1984. *S–C* Mylonites. Journal of Structural Geology 6, 617–638.

Logan, J.M., Rauenzahn, K.A., 1987. Frictional dependence of gouge mixtures of quartz and montmorillonite on velocity, composition and fabric. Tectonophysics 144, 87–108.

Mares, V.M., Kronenberg, A.K., 1993. Experimental deformation of muscovite. Journal of Structural Geology 15, 1061–1075.

Means, W.D., Williams, P.F., 1972. Crenulation cleavage and faulting in an artificial salt–mica schist. Journal of Geology 80, 569–591.

Olgaard, D.L., Evans, B., 1988. Grain growth in synthetic marbles with added mica and water. Contrib. Mineral. Petrol. 100, 246–260.

Passchier, C.W., Trouw, R.A.J., 1996. Microtectonics. Springer-Verlag, Berlin.

Paterson, M.S., 1995. A theory for granular flow accommodated by material transfer via an intergranular fluid. Tectonophysics 245, 135–151.

Platt, J.P., 1984. Secondary cleavages in ductile shear zones. Journal of Structural Geology 6, 439–442.

Platt, J.P., Vissers, R.L.M., 1980. Extensional structures in anisotropic rocks. Journal of Structural Geology 2, 397–410.

Price, R.H., 1982. Effects of anhydrite and pressure on the mechanical behaviour of synthetic rocksalt. Geophysical Research Letters 9, 1029–1032.

Ranalli, G., 1997. Rheology of the lithosphere in space and time. In: Burg, J.-P., Ford, M. (Eds.), Orogeny through Time, Geological Society Special Publication 121, Geological Society Special Publication 54, London, pp. 19–38.

Renard, F., Ortoleva, P., Gratier, J.P., 1997. Pressure solution in sandstones: influence of clays and dependence on temperature and stress. Tectonophysics 280, 257–266.

Ross, J.V., Bauer, S.J., 1992. Semi-brittle deformation of anhydrite–halite shear zones simulating mylonite formation. Tectonophysics 213, 303–320.

Ross, J.V., Wilks, K.R., 1996. Microstructure development in an experimentally sheared orthopyroxene granulite. Tectonophysics 256, 83–100.

Rutter, E.H., 1983. Pressure solution in nature, theory and experiment. Journal of the Geological Society London 140, 725–740.

Rutter, E.H., Brodie, K.H., 1988. The role of tectonic grain size reduction in the rheological stratification of the lithosphere. Geologische Rundschau 77, 295–308.

Rutter, E.H., Mainprice, D.H., 1979. On the possibility of slow fault slip controlled by a diffusive mass transfer process. Gerlands Beitr. Geophysik 88 (2), 154–162.

Shea, W.T., Kronenberg, A.K., 1992. Rheology and deformation mechanisms of an isotropic mica schist. Journal of Geophysical Research 97, 15201–15237.

Shea, W.T., Kronenberg, A.K., 1993. Strength and anisotropy of foliated rocks with varied mica contents. Journal of Structural Geology 15, 1097–1121.

Shimamoto, T., 1986. Transition between frictional slip and ductile flow for halite shear zones at room temperature. Science 231, 711–714.

Shimamoto, T., 1989. The origin of *S–C* mylonites and a new fault-zone model. Journal of Structural Geology 11, 51–64.

Shimamoto, T., Logan, J.M., 1986. Velocity-dependent behavior of simulated halite shear zones: an analog for silicates. In: Das, S., Boatwright, J., Scholz, C.H. (Eds.). Earthquake Source Mechanics. Geophysical Monograph 37, pp. 49–63.

Snoke, A.W., Tullis, J., Todd, V.R., 1999. Fault-related Rocks: A Photographic Atlas. Princeton University Press, Princeton, NJ.

Spiers, C.J., Schutjens, P.M.T.M., Brzesowsky, R.H., Peach, C.J., Liezenberg, J.L., Zwart, H.J., 1990. Experimental determination of constitutive parameters governing creep of rocksalt by pressure solution. In: Knipe, R.J., Rutter, E.H. (Eds.). Deformation Mechanisms, Rheology and Tectonics. Geological Society Special Publication 54, pp. 215–227.

Stewart, M., Holdsworth, R.E., Strachan, R.A., 2000. Deformation processes and weakening mechanisms within the frictional-viscous transition zone of major crustal-scale faults: insights from the Great Glen Fault Zone, Scotland. Journal of Structural Geology 22, 543–560.

Ter Heege, J.H., De Bresser, J.H.P., Spiers, C.J., 1999. The role of microstructure in determining rheology. Geophysical Research Abstracts 1, 69.

White, S.H., Burrows, S.E., Carreras, J., Shaw, N.D., Humphreys, F.J., 1980. On mylonites in ductile shear zones. Journal of Structural Geology 2, 175–187.

Wintsch, R.P., Christoffersen, R., Kronenberg, A.K., 1995. Fluid–rock reaction weakening of fault zones. Journal of Geophysical Research 100, 13021–13032.